Mixed state in antiferromagnetic superconductors

O. Sakai and M. Tachiki
The Research Institute for Iron, Steel and Other Metals, Tohoku University, Katahira, Sendai 980, Japan

T. Koyama,* H. Matsumoto, and H. Umezawa
Department of Physics, The University of Alberta, Edmonton, Alberta T6G 2J1, Canada
(Received 10 June 1981)

The free energy of the mixed state in antiferromagnetic superconductors was derived. The spin magnetic moment induced by the magnetic field of vortices changes drastically at the transition boundary between the antiferromagnetic state and the forced-ferromagnetic state. This effect causes a kink in the curves of the upper and lower critical fields versus temperature at the boundary. When the Néel temperature is very low compared with the superconducting transition temperature, the effect becomes strong enough to cause a dip in the curve of the upper critical field versus temperature. Even in this case the flux density at the upper critical field monotonically decreases with increasing temperature as in usual nonmagnetic superconductors. The present theory well explains the temperature dependence of the upper critical field observed in $DyMo_6S_8$. The magnetization curves were obtained for various cases of parameters.

I. INTRODUCTION

Since the discovery of the coexistence of magnetic and superconducting orders in the rare-earth ternary compounds, much work both experimental and theoretical has been done.[1–3] The antiferromagnetic orders of rare-earth spins coexist with superconductivity in $DyMo_6S_8$, $TbMo_6S_8$, and etc.[4–14] On the other hand, the onset of ferromagnetic order destroys superconductivity in $ErRh_4B_4$ (Refs. 15–17) and $HoMo_6S_8$.[18–21] In a small range of temperature above the ferromagnetic transition temperature of $ErRh_4B_4$ (Refs. 3 and 17) and $HoMo_6S_8$,[20,21] a periodic spin structure with a large wavelength was observed by neutron-diffraction experiments. The temperature dependence of the upper critical field H_{c2} in those magnetic superconductors is anomalous near the magnetic phase transition temperature. In antiferromagnets $DyMo_6S_8$ and $TbMo_6S_8$, the curve of H_{c2} versus temperature has a dip just below the Néel temperature T_N and a maximum near this temperature.[6]

If there exists the strong exchange-type interaction between conduction electrons and rare-earth ions in these compounds, the fluctuation of rare-earth spins acts as a breaker of the Cooper pairs. This pair-breaking effect causes the decrease of the superconducting transition temperature T_c and the upper critical field.[22–29] The spin polarization of conduction electrons induced by the rare-earth magnetization through this interaction may also effect a decrease of H_{c2}.[30,31] However, the experimental results show that the decrease of T_c due to the magnetic rare-earth ions is not so large in most of these compounds.[1,2] The spin-orbit interaction acting on conduction electrons is strong[32] and suppresses the effect of the spin polarization of conduction electrons.[33,34] The band-structure calculation shows that the exchange-type interaction is extremely weak in these ternary compounds, especially in the Chevrel compounds RMo_6S_8,[35] where R represents a rare-earth metal. Therefore, the effect of the exchange-type interaction mentioned above may be renormalized into parameters in these compounds. In this circumstance, the electromagnetic interaction between the persistent current and the rare-earth magnetic moments becomes important.[36] Various unusual phenomena have been predicted from this interaction and some of them have been experimentally confirmed.[37–45]

In antiferromagnets as well as in ferromagnets the electromagnetic interaction becomes important, since the large magnetization of rare-earth ions is induced by the internal magnetic field in the vortices.[46,47] It has been shown in a previous paper that the H_{c2}-versus-temperature curve shows a peak in the antiferromagnetic superconductor equal to that in the ferromagnetic superconductor.[46] In this paper we restricted ourselves to the paramagnetic state above T_N, and H_{c2} was weak enough to neglect the saturation effect of the rare-earth magnetic moments. When the antiferromagnetic components of spins appear below T_N, the ferromagnetic component induced by the applied field is suppressed.[48] If the applied field is very strong, the system changes to the forced-ferromagnetic state. These properties lead to behaviors characteristic in antiferromagnetic superconductors.

We extend the previous theory[46] to the one appli-

cable for antiferromagnetic state by taking account of the saturation effect, and calculate the upper and lower critical fields H_{c2} and H_{c1} as well as the magnetization curves. In our calculation for the antiferromagnetic state, we confine ourselves to the case in which an external magnetic field is applied in the directions parallel and perpendicular to the rare-earth spin axis. Our result is summarized as follows. The H_{c2} curve shows a dip or a cusp at the temperature at which the antiferromagnetic order occurs. This ordering temperature is lower than the Néel temperature at zero field owing to the effect of the internal magnetic field in the vortices. The upper critical field when an external magnetic field is applied parallel to the spin axis increases with decreasing temperature faster than the critical field when the field is applied perpendicular to the spin axis. Even when the H_{c2}-versus-temperature curve shows a dip, the flux density at H_{c2} decreases almost monotonically with increasing temperature. The magnetization curve shows an anomaly at the transition point from the antiferromagnetic state to the forced-ferromagnetic state.

This paper is structured as follows. In Sec. II, the formulation for the Gibbs free energy for the magnetic superconductor is given, and in Sec. III, the expression for the free energy of antiferromagnetic superconductor is given. Finally, in Secs. IV and V numerical results for H_{c1}, H_{c2}, and the magnetization are presented and compared with experiments.

II. FORMULATION

Let us consider a model which consists of superconducting electrons and localized spins. In this model the superconducting electrons interact with the localized spins only through the electromagnetic interaction. The localized spins are coupled through the antiferromagnetic exchange interaction. The energy of the system can be written as[46,49]

$$E = E_0 - \sum_n \vec{b}(\vec{R}_n)\cdot\vec{\mu}(\vec{R}_n) - \tfrac{1}{2}\sum_n\sum_l \gamma_0(\vec{R}_n-\vec{R}_l)\,\vec{\mu}(\vec{R}_n)\cdot\mu(\vec{R}_l) \ , \tag{2.1}$$

where E_0 is the energy of the system of superconducting electrons, the second term is the interaction energy between the microscopic magnetic field $\vec{b}(\vec{x})$ and the magnetic moment $\vec{\mu}(\vec{R}_n)$ located at the site $\vec{R}_n$, and the third term is the exchange energy between the localized spins. $\gamma_0(\vec{R}_n-\vec{R}_l)$ denotes the exchange constant. The free energy can be obtained from (2.1) as

$$F = F_0 - k_B T \sum_n \ln Z(\Lambda(\vec{R}_n)) + \tfrac{1}{2}\sum_n\sum_l \gamma_0(\vec{R}_n-\vec{R}_l)\,\vec{\mu}(\vec{R}_n)\cdot\vec{\mu}(\vec{R}_l) \ . \tag{2.2}$$

In (2.2) the magnetic moment $\vec{\mu}(\vec{R}_n)$ satisfies the equations,

$$\mu(\vec{R}_n) = g\mu_B J B_J\left(\frac{g\mu_B J\Lambda(\vec{R}_n)}{k_B T}\right), \quad \vec{\mu}(\vec{R}_n)\parallel\vec{\Lambda}(\vec{R}_n) \ , \tag{2.3}$$

$$\vec{\Lambda}(\vec{R}_n) = \vec{b}(\vec{R}_n) + \sum_l \gamma_0(\vec{R}_n-\vec{R}_l)\,\vec{\mu}(\vec{R}_l) \ , \tag{2.4}$$

where $B_J(x)$ is the Brillouin function, and $Z(\Lambda(\vec{R}_n))$ is the partition function defined by

$$Z(\Lambda(\vec{R}_n)) = \sinh\left(\frac{2J+1}{2J}\frac{g\mu_B J\Lambda(\vec{R}_n)}{k_B T}\right)\Big/\sinh\left(\frac{1}{2J}\frac{g\mu_B J\Lambda(\vec{R}_n)}{k_B T}\right) \ . \tag{2.5}$$

The quantity F_0 in (2.2) is the free energy of the electron system and has been obtained in the previous paper.[46] In the mixed state, F_0 is expressed as

$$F_0 = -\frac{H_c^2}{8\pi} + W_{\text{core}} + \int d^3x\left[\frac{\vec{b}^2(\vec{x})}{8\pi} - \frac{1}{2c}\vec{j}(\vec{x})\cdot\left(\vec{a}(\vec{x}) - \frac{\hbar c}{e}\vec{\nabla} f(\vec{x})\right)\right] \ . \tag{2.6}$$

In (2.6) the first and second terms represent the superconducting condensation energy and the core energy of vortices, respectively. The persistent current $\vec{j}(\vec{x})$ is expressed as

$$\vec{j}(\vec{x}) = -\frac{c}{4\pi\lambda_L^2(T)}\int d^3y\, c(\vec{x}-\vec{y})\left(\vec{a}(\vec{y}) - \frac{\hbar c}{e}\vec{\nabla} f(\vec{y})\right) \ , \tag{2.7}$$

where $\lambda_L(T)$ and $c(\vec{x})$ are the London penetration depth and the boson characteristic function, respectively, and $\vec{a}(\vec{x})$ is the vector potential related with the microscopic magnetic field $\vec{b}(\vec{x})$ by $\vec{b}(\vec{x})=\vec{\nabla}\times\vec{a}(\vec{x})$. The function $f(\vec{x})$ is equal to half the phase of the superconducting order parameter, and is written for the vortices located at $\vec{\xi}_i$'s as

$$\vec{\nabla}\times\vec{\nabla}f(\vec{x})=\pi\vec{e}_3\sum_i\delta^{(2)}(\vec{x}-\vec{\xi}_i)\ , \tag{2.8}$$

where $\vec{e}_3$ is the unit vector in the direction of the vortices. Substituting (2.7) and (2.8) into the Maxwell equation

$$\vec{\nabla}\times\vec{b}(\vec{x})=\frac{4\pi}{c}\vec{j}(\vec{x})+4\pi\vec{\nabla}\times\vec{m}(\vec{x})\ , \tag{2.9}$$

we obtain

$$-\nabla^2\vec{b}(\vec{x})+\frac{1}{\lambda_L^2(T)}\int d^3y\,c(\vec{x}-\vec{y})\vec{b}(\vec{y})=4\pi\vec{\nabla}\times\vec{\nabla}\times\vec{m}(\vec{x})+\phi\sum_i c(\vec{x}-\vec{\xi}_i)\vec{e}_3\ , \tag{2.10}$$

$$\vec{m}(\vec{x})=\sum_n\delta(\vec{x}-\vec{R}_n)\vec{\mu}(\vec{R}_n)\ , \tag{2.11}$$

ϕ being the unit flux $hc/2e$.

Equations (2.3), (2.4), and (2.10) determine $\vec{\mu}(\vec{R}_n)$ and $\vec{b}(\vec{x})$ in the mixed state. Let us introduce the internal magnetic field $\vec{h}(\vec{x})$ defined by

$$\vec{h}(\vec{x})=\vec{b}(\vec{x})-4\pi\vec{m}(\vec{x})\ . \tag{2.12}$$

The field $\vec{h}(\vec{x})$ satisfies the equation

$$\vec{j}(\vec{x})=\frac{c}{4\pi}\vec{\nabla}\times\vec{h}(\vec{x})\ . \tag{2.13}$$

Then the free energy can be expressed in terms of $\vec{h}(\vec{x})$ as

$$F=-\frac{H_c^2}{8\pi}+W_{\text{core}}+\int d^3x\left(\frac{\phi}{8\pi}\sum_i\vec{e}_3\cdot\vec{h}(\vec{\xi}_i)\delta^{(2)}(\vec{x}-\vec{\xi}_i)+\frac{1}{2}\vec{h}(\vec{x})\cdot\vec{m}(\vec{x})\right)$$
$$-k_BT\sum_n\ln Z(\Lambda(\vec{R}_n))+\frac{1}{2}\sum_n\sum_l\vec{\mu}(\vec{R}_n)\gamma(\vec{R}_n-\vec{R}_l)\vec{\mu}(\vec{R}_l)\ . \tag{2.14}$$

Here $\gamma(\vec{R}_n-\vec{R}_l)$ is the spin-spin interaction which includes the dipole interaction. The component of $\gamma(\vec{R}_n-\vec{R}_l)$ is given by

$$\gamma_{ij}(\vec{R}_n-\vec{R}_l)=\gamma_0(\vec{R}_n-\vec{R}_l)\delta_{ij}+4\pi\int\frac{d^3k}{(2\pi)^3}\left(\delta_{ij}-\frac{k_ik_j}{k^2}\right)\exp[i\vec{k}\cdot(\vec{R}_n-\vec{R}_l)]\ . \tag{2.15}$$

This interaction is the spin-spin interaction in the normal state.

In a given external field the relevant thermodynamic potential is the Gibbs free energy. The Gibbs free energy for the mixed state is obtained from F by using the Legendre transformation

$$G_{\text{mix}}=F-\frac{n\phi}{4\pi}H\ , \tag{2.16}$$

where $n\phi$ is the flux density and H is the external magnetic field. The free energy (2.14) is the function of the vortex density n. Using the condition $\partial G_{\text{mix}}/\partial n=0$, we have the relation between n and H,

$$\frac{4\pi}{\phi}\frac{\partial F}{\partial n}-H=0\ . \tag{2.17}$$

With use of the relation, the Gibbs free energy is written as

$$G_{\text{mix}}=F-n\frac{\partial F}{\partial n}\ . \tag{2.18}$$

The upper and lower critical fields H_{c2} and H_{c1} can be calculated by the method in Ref. 46.

III. GIBBS FREE ENERGY AND UPPER CRITICAL FIELD

In this section we calculate the expression of the Gibbs free energy and obtain the upper and lower critical fields. By solving (2.3) and (2.10) we obtain $\vec{b}(\vec{x})$ and $\vec{m}(\vec{x})$ for the mixed state of antiferromagnetic superconductors. The solution depends on the direction of the vortices relative to the spin axis. In the following we confine ourselves to the case in which the applied field is either perpendicular or parallel to the easy axis of the sublattice magnetization.

First we assume that an external magnetic field is applied in the direction perpendicular to the easy axis. When the field is weak and the temperature is lower than T_N, the sublattice magnetization is tilted from

the easy axis.[48] As the field increases, the tilted angle increases and at a critical field the transition from the antiferromagnetic state to the forced-ferromagnetic state occurs. The critical field for this transition is shown schematically by the dot-dashed curve in Fig. 1(a). The antiferromagnetic state is denoted by A and the ferromagnetic state by F.

In the region A, we can put $\vec{\mu}(\vec{R}_n)$ and $\vec{h}(\vec{R}_n)$ in the form

$$\vec{\mu}(\vec{R}_n)=[\mu_0+\tilde{\mu}_1(\vec{R}_n)]\vec{e}_1 + [\mu_{\vec{Q}}e^{i\vec{Q}\cdot\vec{R}_n}+\tilde{\mu}_3(\vec{R}_n)]\vec{e}_3 \ , \tag{3.1}$$

$$\vec{h}(\vec{R}_n)=[h_0+\tilde{h}_1(\vec{R}_n)]\vec{e}_1 + [\vec{h}_{\vec{Q}}e^{i\vec{Q}\cdot\vec{R}_n}+\tilde{h}_3(\vec{R}_n)]\vec{e}_3 \ . \tag{3.2}$$

Here $\vec{e}_1$ and $\vec{e}_3$ are the unit vectors perpendicular and parallel to the easy axis, respectively, μ_0 and $\mu_{\vec{Q}}$ are the uniform and antiferromagnetic components of the spin magnetic moment, respectively, and h_0 and $h_{\vec{Q}}$ are those of the internal magnetic field. The quantities with tilde represent the deviations from the average values μ_0 and $\mu_{\vec{Q}}$, etc. Substituting (3.1) and (3.2) into (2.3), (2.4), and (2.10) and expanding the equation up to first order of the deviations, we can get the following relations which determine the average values and the Fourier components of the deviations with wave numbers corresponding to the reciprocal vectors of the flux line lattice:

$$m_0=h_0/[\Gamma(\vec{Q})-\Gamma(0)] \ , \tag{3.3}$$

$$m=(m_0^2+m_{\vec{Q}}^2)^{1/2} =Ng\mu_B JB_J(g\mu_B J\Lambda_\perp/k_BT) \ , \tag{3.4}$$

$$\tilde{h}(\vec{K})=\frac{\lambda_L^{-2}(T)c_K n\phi}{K^2+[1+4\pi\chi_\perp(\vec{K})]\lambda_L^{-2}(T)c_K} \ , \tag{3.5}$$

$$\tilde{m}(\vec{K})=\chi_\perp(\vec{K})\tilde{h}(\vec{K}) \ , \tag{3.6}$$

with $m_0=N\mu_0$ and $m_{\vec{Q}}=N\mu_{\vec{Q}}$. Here $\Gamma(\vec{k})$ is the transverse component of the Fourier transform of the exchange constant

$$\gamma(\vec{k})=\int d^3r\,\gamma(\vec{r})\exp(-i\vec{k}\cdot\vec{r}) \ .$$

The molecular field in (3.4) is given by $\Lambda_\perp=\Gamma_{\vec{Q}}m$.

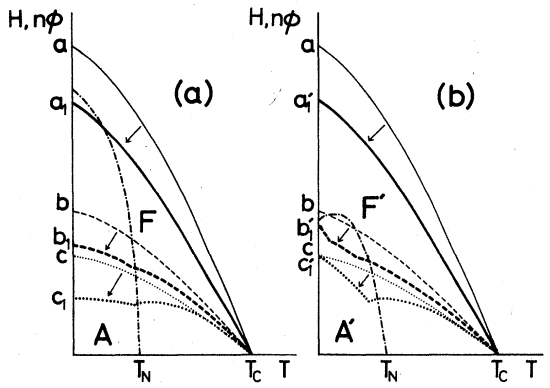

FIG. 1. Schematic diagrams of the critical flux density. The boundary between the antiferromagnetic and the forced-ferromagnetic state is indicated by the dot-dashed curve. (a) $\vec{H}_\perp$ easy axis and (b) $\vec{H}\|$ easy axis. The curves a, b, and c show typical temperature dependence of the critical flux density. The curves a_1 and a_1' are the H_{c2} curves for the same parameters as those for the curve a, and so on.

The magnetic susceptibility $\chi_\perp(\vec{k})$ is calculated as

$$\chi_\perp(\vec{k})=\left[\Gamma(\vec{Q})-\Gamma(\vec{k}) + \frac{m_0^2(\Gamma(\vec{Q})-\Gamma(\vec{k}-\vec{Q}))}{m_{\vec{Q}}^2+\sigma_{\vec{Q}}m^2(\Gamma(\vec{Q})-\Gamma(\vec{k}-\vec{Q}))}\right]^{-1} , \tag{3.7}$$

$$\sigma_{\vec{Q}}=\frac{C\alpha_J^{\vec{Q}}}{T-C\Gamma(\vec{Q})\alpha_J^{\vec{Q}}} \ , \qquad \alpha_J^{\vec{Q}}=\frac{3J}{J+1}B_J'\left(\frac{g\mu_B J\Lambda_\perp}{k_BT}\right) \ . \tag{3.8}$$

The function c_k is the Fourier transform of the boson characteristic function, and C is the Curie constant $N(g\mu_B)^2J(J+1)/3k_B$. In (3.5) and (3.6) we abbreviated suffix 1 of $\tilde{h}_1(\vec{K})$ and $\tilde{m}_1(\vec{K})$, and neglected $\tilde{h}_3(\vec{K})$ and $\tilde{m}_3(\vec{K})$ since they are very small. The boundary between the regions A and F is determined by the condition of an infinitesimal $m_{\vec{Q}}$. Therefore, from (2.12), (3.3), and (3.4), the flux density at this boundary is given by

$$n_\perp\phi=[\Gamma(\vec{Q})-\Gamma(0)+4\pi]m \ . \tag{3.9}$$

We can obtain the relations for the average values and the deviations of the magnetization and the internal field in the forced-ferromagnetic state in a similar way. The results are given as follows:

$$m_0=Ng\mu_B JB_J(g\mu_B J\Lambda_f/k_BT) \ , \tag{3.10}$$

with $\Lambda_f=h_0+\Gamma(0)m_0$ and $m_{\vec{Q}}=0$. The magnetic

susceptibility is written as

$$\chi_f(\vec{k}) = \frac{C\alpha_J}{T - C\Gamma(\vec{k})\alpha_J} , \tag{3.11}$$

$$\alpha_J = \frac{3J}{2J+1} B_J'\left(\frac{g\mu_B J \Lambda_f}{k_B T}\right) . \tag{3.12}$$

By replacing $\chi_\perp(\vec{K})$ in (3.5) and (3.6) by $\chi_f(\vec{K})$, the deviations $\tilde{h}(\vec{K})$ and $\tilde{m}(\vec{K})$ in this case are obtained.

Next we consider the case in which the magnetic field is applied parallel to the easy axis. The magnetic moments on the two sublattices have the same magnitude but are in the opposite direction to each other in the absence of vortices. In the presence of vortices the magnitude of the magnetic moment varies from site to site. When the flux density increases further over a certain critical value, the antiferromagnetic components disappear. In Fig. 1(b) the boundary between the antiferromagnetic region A' and the forced-ferromagnetic region F' is illustrated schematically by the dot-dashed curve. The critical field at $T=0$ becomes half the value in the field perpendicular to the easy axis.

In the region A' the local magnetization and the local magnetic field are written in the form

$$\vec{\mu}(\vec{R}_n) = [\mu_0 + \mu_{\vec{Q}} e^{i\vec{Q}\cdot\vec{R}_n} + \tilde{\mu}(\vec{R}_n)]\vec{e}_3 , \tag{3.13}$$

$$\vec{h}(\vec{R}_n) = [h_0 + h_{\vec{Q}} e^{i\vec{Q}\cdot\vec{R}_n} + \tilde{h}(\vec{R}_n)]\vec{e}_3 . \tag{3.14}$$

We can obtain the relations for m_0 and $m_{\vec{Q}}$ by following the similar procedure to obtain (3.3) and (3.4)

$$m_0 + m_{\vec{Q}} = Ng\mu_B J B_J\left(\frac{g\mu_B J \Lambda_{\parallel}(+)}{k_B T}\right) , \tag{3.15}$$

$$m_0 - m_{\vec{Q}} = Ng\mu_B J B_J\left(\frac{g\mu_B J \Lambda_{\parallel}(-)}{k_B T}\right) , \tag{3.16}$$

with $\Lambda_{\parallel}(\pm) = h_0 + \Gamma(0)m_0 \pm \Gamma(\vec{Q})m_{\vec{Q}}$. The magnetic susceptibility is given by

$$\chi_{\parallel}(\vec{k}) = \frac{C\{T\alpha_J(+) - C\Gamma(\vec{k}+\vec{Q})[\alpha_J^2(+) - \alpha_J^2(-)]\}}{[T - C\alpha_J(+)\Gamma(\vec{k})][T - C\alpha_J(+)\Gamma(\vec{k}+\vec{Q})] - C^2\alpha_J^2(-)\Gamma(\vec{k})\Gamma(\vec{k}+\vec{Q})} , \tag{3.17}$$

$$\alpha_J(\pm) = \frac{1}{2}\frac{3J}{J+1}\left[B_J'\left(\frac{g\mu_B J\Lambda_{\parallel}(+)}{k_B T}\right) \pm B_J'\left(\frac{g\mu_B J\Lambda_{\parallel}(-)}{k_B T}\right)\right] . \tag{3.18}$$

The deviations $\tilde{h}(\vec{K})$ and $\tilde{m}(\vec{K})$ have forms similar to (3.5) and (3.6).

In the region F', the solution is determined from the same equations as those used in the region F; (3.10)–(3.12). The flux density, $n_{\parallel}\phi$ at the boundary between the regions A' and F' is calculated by taking the limit of $m_{\vec{Q}} = 0$ in (3.15) and (3.16). The equation to determine $n_{\parallel}$ is

$$1 = \Gamma(\vec{Q})\frac{C}{T}\frac{3J}{J+1} B_J'\left(\frac{g\mu_B J\Lambda_f}{k_B T}\right) , \tag{3.19}$$

with $\Lambda_f = n_{\parallel}\phi + [\Gamma(0) - 4\pi]m_0$, where m_0 is calculated from (3.10).

In the above discussion we assumed strong anisotropy. However when the anisotropy is weak the spin-flop transition occurs at a critical field below the field at the A'-F' boundary.[48] At the spin-flop transition the sublattice magnetization rotates suddenly, and take a configuration almost perpendicular to the magnetic field. The magnetization and the susceptibility in the spin-flopped state are almost equal to those in the antiferromagnetic state A as long as the anisotropy energy is small. In this paper we neglect the spin-flop transition for simplicity.

The free energy F is obtained from (2.14) by using the results (3.3)–(3.18) as

$$F = -\frac{H_c^2}{8\pi} + W_{\text{core}} + \frac{n\phi}{8\pi}h_0 + \frac{n\phi}{8\pi}\sum_{\vec{K}\neq 0}\tilde{h}(\vec{K}) + \tfrac{1}{2}h_0 m_0 + \tfrac{1}{2}\Gamma(0)m_0^2 + \tfrac{1}{2}\Gamma(\vec{Q})m_{\vec{Q}}^2 - \tfrac{1}{2}Nk_B T\sum_{\nu=\pm 1}\ln Z(\Lambda(\nu)) , \tag{3.20}$$

with

$$\Lambda(\pm) = \begin{cases} \Lambda_\perp \text{ for the state } A & (3.21) \\ \Lambda_{\parallel}(\pm) \text{ for the state } A' & (3.22) \\ \Lambda_f \text{ for the states } F \text{ and } F' . & (3.23) \end{cases}$$

The core energy W_{core} is given by

$$W_{\text{core}} = n\left[E_1 - E_2\sum_{i(\neq 0)} b(\vec{\xi}_i)\right] \tag{3.24}$$

$$= n\left[E_1 - E_2\left[n\phi + \sum_{\vec{K}\neq 0}\vec{b}(\vec{K}) - b(\vec{x}=0)\right]\right] , \tag{3.25}$$

where E_1 is the normal core energy for an isolated vortex,

$$E_1=\hbar^2c^2/32e^2\lambda_L^2(T) \ , \tag{3.26}$$

and E_2 is a parameter determined from the thermodynamical conditions.[46]

Using (2.17) and (2.18), we have the expressions for the thermodynamical field H and the Gibbs free energy $G_{\rm mix}$

$$H=h_0+\frac{4\pi}{\phi}\frac{\partial W_{\rm core}}{\partial n}+\frac{1}{2}\left[1+n\frac{\partial}{\partial n}\right]\sum_{\vec{K}\neq 0}\tilde{h}(\vec{K}) \ , \tag{3.27}$$

$$G_{\rm mix}=-\frac{H_c^2}{8\pi}-\frac{h_0^2}{8\pi}+\left[1-n\frac{\partial}{\partial n}\right]W_{\rm core} -\frac{n^2\phi}{8\pi}\frac{\partial}{\partial n}\sum_{\vec{K}\neq 0}\tilde{h}(\vec{K})+G_m \ , \tag{3.28}$$

$$G_m=\tfrac{1}{2}\Gamma(0)m_0^2+\tfrac{1}{2}\Gamma(\vec{Q})m_{\vec{Q}}^2 -\tfrac{1}{2}Nk_BT\sum_{\nu=\pm}\ln Z(\Lambda(\nu)) \ . \tag{3.29}$$

If h_0 included in $\Lambda(\nu)$ in (3.29) is replaced by H, the Gibbs free energy for the normal state is expressed as

$$G_{\rm normal}=-\frac{H^2}{8\pi}+G_m \ . \tag{3.30}$$

The equations to determine n_c and E_2 are

$$\frac{\partial W_{\rm core}}{\partial n}+\frac{\phi}{8\pi}\left[1+n\frac{\partial}{\partial n}\right]\sum_{\vec{K}\neq 0}\tilde{h}(\vec{K})=0 \ , \tag{3.31}$$

$$-\frac{H_c^2}{8\pi}+\left[1-n\frac{\partial}{\partial n}\right]W_{\rm core}-\frac{n^2\phi}{8\pi}\frac{\partial}{\partial n}\sum_{\vec{K}\neq 0}\tilde{h}(\vec{K})=0 \ . \tag{3.32}$$

The upper critical field H_{c2} is expressed by the relation

$$H_{c2}=n_c\phi-4\pi m_0(n_c) \ . \tag{3.33}$$

In our numerical calculation we used the following form for the boson characteristic function:

$$c_k=\exp\{-\nu[\bar{k}/\kappa(t)]^\eta\} \ , \tag{3.34}$$

$$\bar{k}=\lambda_L(T)k \ , \tag{3.35}$$

$$\kappa(t)=\kappa_B[\lambda_L(T)/\lambda_L(0)]/\gamma(t) \ , \tag{3.36}$$

$$\gamma(t)=1+at^n(1-t)^{-m} \ , \tag{3.37}$$

$$\nu=-0.4257VN(0)+0.559 \ , \tag{3.38}$$

$$\eta=-0.7857VN(0)+2.207 \ , \tag{3.39}$$

$$a=-0.0536VN(0)+0.3719 \ , \tag{3.40}$$

$$n=0.3714VN(0)+3.846 \ , \tag{3.41}$$

$$m=-0.0414VN(0)+0.556 \ . \tag{3.42}$$

Here $VN(0)$ is the BCS coupling constant, and t is the normalized temperature $t=T/T_c$. The temperature dependence of the London penetration depth is obtained from the relation

$$\left[\frac{\lambda_L(0)}{\lambda_L(T)}\right]^2=1+2\int d\delta\frac{\partial f_E}{\partial E} \ , \tag{3.43}$$

where $f_E=[\exp(E/k_BT)+1]^{-1}$ and $E=[\delta^2+\Delta(T)^2]^{1/2}$, $\Delta(T)$ being the energy gap. The exchange constant $\Gamma(\vec{k})$ is approximated by $\Gamma(\vec{k})\cong\Gamma(0)=T_m/C$ for small $|\vec{k}|$ and $\Gamma(\vec{k})\cong\Gamma(\vec{Q})=T_N/C$ for small $|\vec{k}-\vec{Q}|$. The temperatures T_m and T_N are, respectively, the paramagnetic Curie temperature and the Néel temperature. The parameters used in our calculations are

$$\kappa_B,\ VN(0),\ J,\ t_N=T_N/T_c,\ t_m=T_m/T_c \ , \quad c=4\pi C/T_N,\ u=Ng\mu_BJ/[\phi/\lambda_L^2(0)] \ . \tag{3.44}$$

The results of numerical calculations are given in Secs. IV–VI.

IV. NUMERICAL RESULTS FOR CRITICAL FIELDS

In this section we present the calculated results of H_{c1} and H_{c2} and compare them with experiments. As seen from (2.10) and (2.12), the flux density in the magnetic superconductor is given by $n\phi=h_0+4\pi m_0$, which indicates that the induced-spin magnetic moment m_0 contributes to the magnetic induction $b_0=n\phi$. For an external field near H_{c2} and for a large κ_B, the inhomogeneous components of the magnetic field, the magnetic induction and the spin magnetization $\tilde{h}(\vec{x})$, $\tilde{b}(\vec{x})$, and $\tilde{m}(\vec{x})$ are very small. If we can neglect those in (3.27) and (3.28) we obtain a relation $n_c\phi\sim H_{c2}^0(T)$, where $H_{c2}^0(T)$ is the fictitious upper critical field when the sample has no spin magnetization. Combining this relation with (3.33), the upper critical field can be estimated approximately from the relation

$$H_{c2}(T)\sim H_{c2}^0(T)-4\pi m_0 \ , \tag{4.1}$$

where m_0 is the spin magnetization at H_{c2}.

The spatial dependence of the magnetic field of vortex is affected by the spin magnetization as seen from (3.5), and the inversion of the field direction occurs in some portion of the vortex near the Néel temperature. Through this effect, the magnetic superconductor has a tendency to become a type-I or a type-II-1 superconductor.[46,50]

First we consider the case of $\vec{H}$ perpendicular to the easy axis of spins. When the superconducting transition temperature T_c is higher than the Néel temperature T_N, there are the following two cases. The curve of $n_c\phi$ crosses the A-F boundary as shown by the curves b and c in Fig. 1(a), and the curve of $n_c\phi$ does not cross the A-F boundary as shown by

the curve a in Fig. 1(a). The latter corresponds to the case for large κ_B.

Let us consider the case of the curve b in Fig. 1(a). In the region A, H_{c2} is estimated from (3.3) and (4.1) as

$$H_{c2}(T) \sim H_{c2}^0(T)\{1+4\pi/[\Gamma(\vec{Q})-\Gamma(0)]\}^{-1} .$$

The field $H_{c2}(T)$ increases gradually as T decreases, since $H_{c2}^0(T)$ increases. The induced-spin magnetic moment m_0 under a fixed magnetic field is constant independent of T in the region A. On the other hand in the region F, it becomes large as T decreases under a fixed mangetic field. Reflecting this feature, $H_{c2}(T)$ is depressed more from $H_{c2}^0(T)$ as T decreases in the region F. When the decrease of $H_{c2}(T)$ from $H_{c2}^0(T)$ overcomes the increase of $H_{c2}^0(T)$, $H_{c2}(T)$ decreases as T decreases in the region F, and then show a dip at the temperature of the antiferromagnetic order setting in. The H_{c2}-versus-T curve of this type is expected in the case of T_N much lower than T_c, since when T decreases near T_N, $H_{c2}^0(T)$ scarcely changes, but the induced-spin magnetic moment rapidly increases.

We introduce a parameter defined by $\epsilon_0=(T_N-T_m)/T_N$.[46] The calculated result of $H_{c2}(T)$ for the case of $\kappa_B=2.5$ and $t_N=0.15$ and for various values of ϵ_0 are shown in Fig. 2. At a temperature where the curve of $n_c\phi$ crosses the A-F boundary the H_{c2}-versus-T curve shows a dip. As seen from the expression $H_{c2}(T) \sim H_{c2}^0(1+c/\epsilon_0)^{-1}$ in the region A, $H_{c2}(T)$ is strongly depressed when ϵ_0 decreases. It is

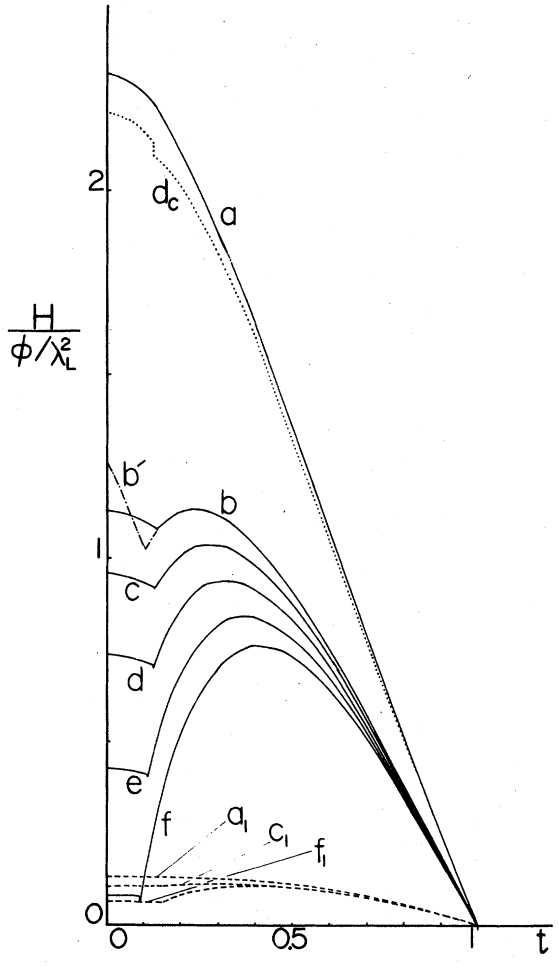

FIG. 2. H_{c2} and H_{c1} for $t_N=0.15$, $\kappa_B=2.5$, $c=2$, and $u=0.1$. a and a_1 are H_{c2}^0 and H_{c1}^0 for the nonmagnetic superconductor, respectively. b, c, d, e, and f are H_{c2} for $\epsilon_0=2$, 1.5, 1, 0.5, and 0.1, respectively, and c_1 and f_1 are H_{c1} for $\epsilon_0=1.5$ and 0.1, respectively, in $\vec{H}\perp$ easy axis. d_c is the critical flux density $n_c\phi$ for $\epsilon_0=1$ in $\vec{H}\perp$ easy axis. b′ is H_{c2} for $\epsilon_0=2$ in $\vec{H}\parallel$ easy axis.

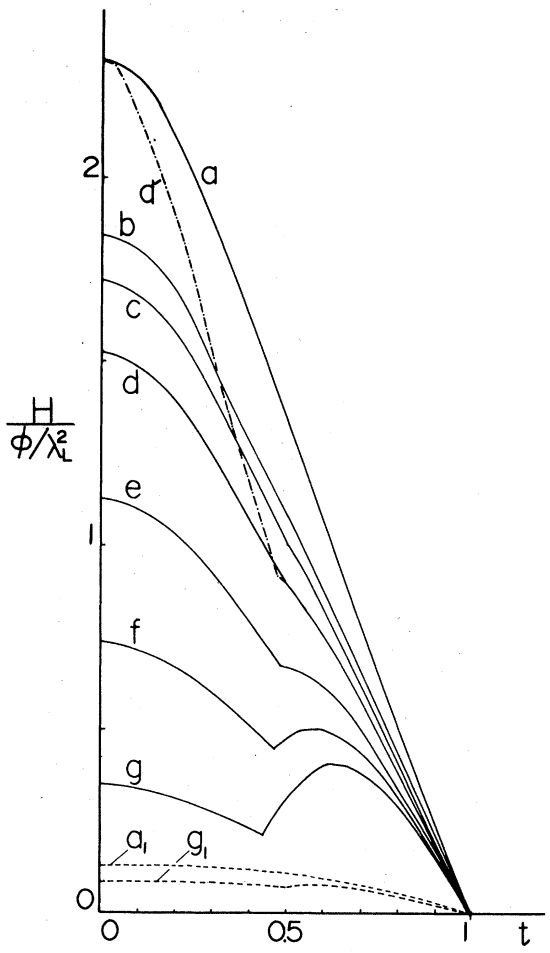

FIG. 3. H_{c2} and H_{c1} for $t_N=0.5$, $\kappa_B=2.5$, $c=2$, and $u=0.1$. a and a_1 are H_{c2}^0 and H_{c1}^0 for nonmagnetic superconductor, respectively. b, c, d, e, f, and g are H_{c2} for $\epsilon_0=2$, 1.5, 1, 0.5, 0.25, and 0.1, respectively, and g_1 is H_{c1} for $\epsilon_0=0.1$ in $\vec{H}\perp$ easy axis. d′ is H_{c2} for $\epsilon_0=1$ in $\vec{H}\parallel$ easy axis.

seen from the curves d and d_c in Fig. 2 that even if $H_{c2}(T)$ is strongly depressed, the critical flux density $n_c\phi = H_{c2}(T) + 4\pi m_0$ is approximately equal to $H_{c2}^0(T)$. The lower critical field H_{c1} defined by the limit of $n=0$ is given by $H_{c1}(T) = \frac{1}{2}h(0) + 4\pi E_1/\phi$. For large κ_B this expression is written as $H_{c1}^0(T)\ln[\kappa_B^2/(1+4\pi\chi)+1]/\ln(\kappa_B^2+1)$. When the transition at H_{c1} is of first order, the observed $H_{c1}(T)$ is slightly lower than the value defined above. The field $H_{c1}(T)$ shown by the dashed curves in Fig. 2 reveals a mild kink very near T_N.

In Fig. 3, we show the calculated results of H_{c2} for the case of $t_N = 0.5$. There appears a dip or a kink when c/ϵ_0 is very large.

Figure 4 shows the fields H_{c1} and H_{c2} for several values of κ_B. Curves b and c denote $H_{c2}(T)$ when $n_c\phi$ curves do not cross the A-F boundary. In this case the H_{c2} curve has no kink. However the curve decreases near absolute zero when $n_c\phi$ is very near the A-F boundary as seen from the curve c.

When T_N is higher than T_c, we expect two possible cases. In a case that the $n_c\phi$ curve crosses the A-F boundary the H_{c2} curve show a kink. On the other-hand, when the $n_c\phi$ curve is entirely inside the region A, the H_{c2} curve has no kink.

Next we consider the case of $\vec{H}$ parallel to the easy axis. In the antiferromagnetic region A' in Fig. 1(b), under a fixed magnetic field m_0 decreases as T decreases and vanishes at $T=0$. Thus H_{c2} increases and reaches $H_{c2}^0(T)$ at $T=0$ as long as $n_c\phi$ is smaller than the critical field for the A'-F' boundary. Figure 1(b) shows typical types of H_{c2} curves. Curve a corresponds to the case that the $n_c\phi$ curve does not cross the boundary, curve c to the case that the $n_c\phi$ curve crosses the boundary once, and curve b to the case that the $n_c\phi$ curve crosses the boundary twice. The dot-dashed curve d′ in Fig. 4 corresponds to the second case, and curve b′ in Fig. 2 to the third case.

In Fig. 5, we show the experimental values of H_{c2} for $DyMo_6S_8$ by solid circles[6] and the calculated values by the solid curve. For the calculation we chose the parameters as shown in the figure captions and assumed the case of $\vec{H}$ perpendicular to the easy axis. The calculated value of the spin magnetization m_0 at H_{c2} is shown by the dashed curve.

Recent neutron scattering experiments at $T=0.19$ K shows that the ferromagnetic component of spins increases with increasing H and that some amount of antiferromagnetic ordering survives even at H_{c2}.[14] Measurements of the dc susceptibility in the paramagnetic normal state indicate that T_m is positive in $DyMo_6S_8$.[51] These experimental data are consistent

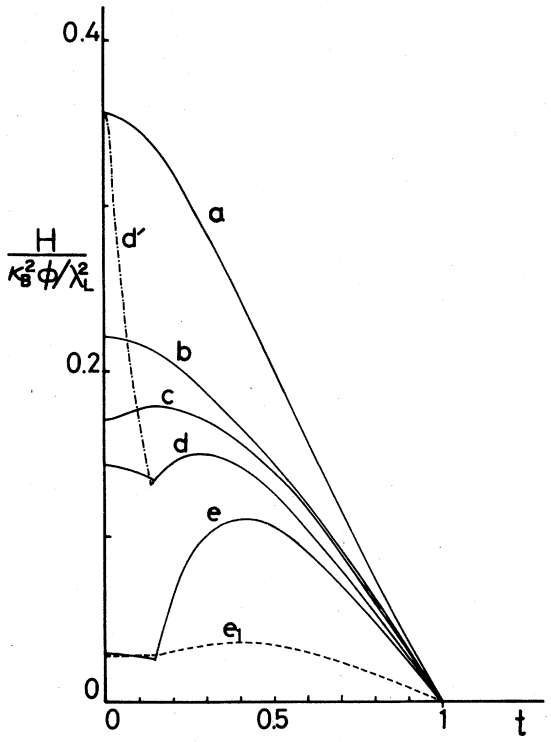

FIG. 4. H_{c2} and H_{c1} for $t_N=0.15$, $c=2.0$, and $u=0.1$ for various values of κ_B. The fields are normalized by a factor κ_B^2. a is H_{c2}^0 for $\kappa_B=1.5$. b, c, d, and e are H_{c2} for ($\epsilon_0=1$, $\kappa_B=4$), ($\epsilon_0=1$, $\kappa_B=3.5$), ($\epsilon_0=1.5$, $\kappa_B=1.5$), and ($\epsilon_0=0.25$, $\kappa_B=1.5$), respectively, and e_1 is H_{c1} for ($\epsilon_0=0.25$, $\kappa_B=1.5$) in $\vec{H}\perp$ easy axis. d′ is H_{c2} for ($\epsilon_0=1.5$, $\kappa_B=1.5$) in $\vec{H}\parallel$ easy axis.

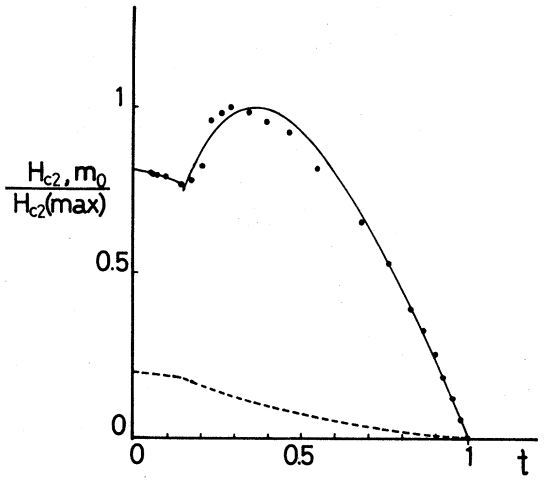

FIG. 5. H_{c2} for $DyMo_6S_8$. The field H_{c2} and m_0 are normalized by the maximum value of H_{c2}, $H_{c2}(\max)$. The solid circles are the experimental data of H_{c2} by Ishikawa *et al.*, and the solid curve is the calculated value of H_{c2}. The dashed curve is the calculated value of m_0 at H_{c2}. The parameters $\kappa_B=2$, $u=0.1$, and $c=2.4$ are used. t_m is chosen to be 0.07 from experimental data in Ref. 51, and t_N is chosen to be 0.23. $H_{c2}(\max)$ is calculated to be $0.416[\phi/\lambda_L^2(0)]$, which is 1.5 kOe in the experiments.

with choice of the parameters used in Fig. 5. In the case of $GdMo_6S_8$ (Ref. 10) and $TbMo_6S_8$,[6] the experimental upper critical fields show a rapid increase with decreasing temperature after they pass a dip which appears at a temperature slightly below T_N.[2] The H_{c2} behavior is similar to that of the curves d′ and f in Fig. 3. Recently in $Er(Rh_xRu_{1-x})_4B_4$ and $Ho(Rh_xRu_{1-x})_4B_4$ the H_{c2} behavior similar to the curves c and d in Fig. 2 were observed.[52]

V. MAGNETIZATION

The magnetization[7] in the superconducting phase is calculated from the expression $M=(4\pi)^{-1}(n\phi-H)$. The magnetization increases with H above H_{c1} and becomes positive in high fields, since the paramagnetic contribution from the spin magnetization exceeds the diamagnetic contribution.

In Fig. 6, we show the magnetization curve when we use the same parameters as those for the curve d in Fig. 4. At H_{c2} indicated by the solid circles on the curves the slope of M decreases slightly because the diamagnetic contribution vanishes there. In the field perpendicular to the easy axis, the magnetization curves are of the type-II-1 superconductor at low temperatures. Since the spin magnetic susceptibility does not depend on T in the antiferromagnetic region, M seems to be almost temperature independent for $T < T_N$ except very near T_N. On the other hand in the field parallel to the easy axis the spin magnetization decreases as T is lowered, and therefore M decreases with decreasing temperature and tends to magnetization for the nonmagnetic superconductor as

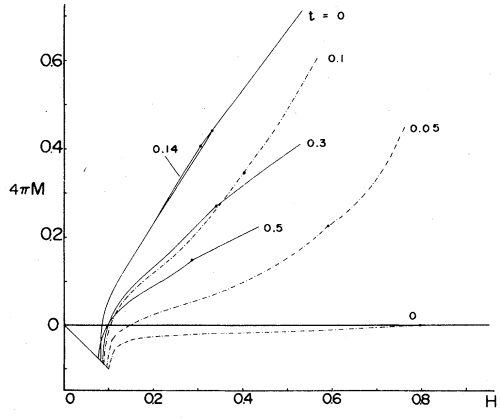

FIG. 6. Magnetization curves for $t_N=0.15$, $\kappa_B=1.5$, $c=2$, $u=0.1$, and $\epsilon_0=1.5$. The solid circles on the curves denote H_{c2}. The solid curves are magnetization in $\vec{H}\perp$ easy axis, and the dot-dashed curves in $\vec{H}\parallel$ easy axis. M and H are given in units of $\phi/\lambda_L^2(0)$. The temperatures are indicated in the figures.

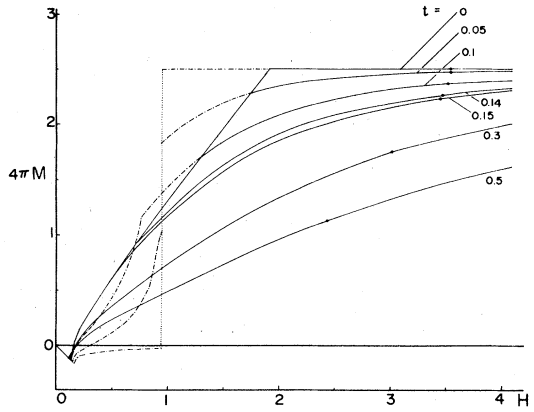

FIG. 7. Magnetization curves for $t_N=0.15$, $\kappa_B=4$, $c=2$, $u=0.1$, and $\epsilon_0=1.5$. See the caption of Fig. 6.

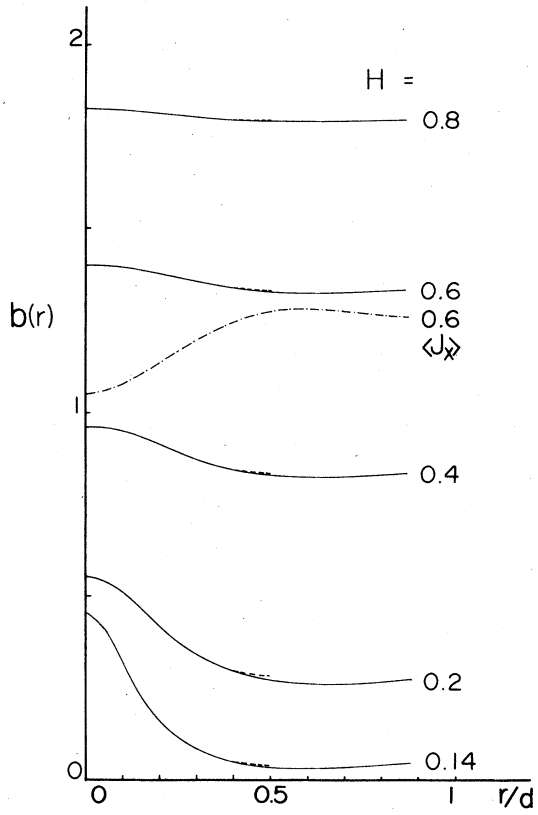

FIG. 8. Spatial variation of $b(r)$ for $t_N=0.15$, $\kappa_B=4$ $c=2$, $u=0.1$, $\epsilon_0=1.5$, and $t=0.14$ in $\vec{H}\perp$ easy axis. For these parameters $H_{c1}=0.135$ and $H_{c2}=3.551$. $b(r)$ and H are normalized by units of $\phi/\lambda_L^2(0)$. d is the nearest-neighbor distance of the vortex lattice. Solid curves shows $b(r)$ along the line to a second-neighbor point and the dashed curves shows $b(r)$ along the line to a nearest-neighbor point. The dot-dashed curve shows the component of spin $\langle J_x\rangle$ perpendicular to the external field for $H=0.6$, where the magnitude of spin $\langle|\vec{J}|\rangle$ is 2.6.

temperature goes to absolute zero.

Figure 7 shows the magnetization curves for the case that H_{c2} is larger than the critical field for the antiferromagnetic to the forced-ferromagnetic transition. In the field perpendicular to the easy axis and at absolute zero, M increases with H up to the A-F transition. Above the transition M is almost saturated. For finite temperatures the critical field for the A-F transition decreases from the field at absolute zero. In the field parallel to the easy axis, M at absolute zero is equal to that of the nonmagnetic superconductor for H weaker than the critical field of the A'-F' boundary. At the field M suddenly jumps to the magnetization in the region F'.

The local magnetic induction , $b(\vec{r})$ is shown in Fig. 8. When H is very near H_{c1}, $b(\vec{r})$ strongly varies in space. However as H increases a little from H_{c1}, $b(\vec{r})$ becomes immediately homogeneous. Periodic variations of $b(\vec{r})$ and the sublattice magnetization under a field very near H_{c1} may be detected by neutron-diffraction experiments.

VI. DISCUSSION

In the preceding sections we have shown that the critical flux density $n_c\phi = H_{c2} + 4\pi m_0$ is not so strongly affected from the spin magnetic moment and is nearly equal to the upper critical field of the nonmagnetic superconductor $H_{c2}^0(T)$.[53] We have neglected in this paper the effect of the exchange-type interaction between conduction electrons and rare-earth ions.[54–59] In Sec. I, we discussed that this interaction is weak in the Chevrel compounds.

However if there exist the strong exchange-type interaction, the pair-breaking effect through this interaction causes the decrease of the superconducting condensation energy, and thus the decrease of the critical flux density.[23,27] The gap formation at the Fermi surface due to the antiferromagnetic spin ordering through this interaction,[58] as well as the spin polarization of conduction electrons induced by the spin magnetization through this interaction, may also cause the decrease of the critical flux density. The decrease of the critical flux density will show an abrupt change at the temperature of the antiferromagnetic order setting in.

A part of the decrease of H_{c2} due to the magnetic ions in the rhodium boride compounds may be ascribed to the effect of the exchange-type interaction,[58] since $4\pi m_0$ for $ErRh_4B_4$ is considerably smaller than the upper critical field of a nonmagnetic superconductor $LuRh_4B_4$.[60]

ACKNOWLEDGMENTS

The authors would like to express their sincere thanks to Professor A. Kotani at Osaka University, and to Dr. S. Maekawa and Mr. S. Takahashi for valuable discussions, and to Mr. R. Teshima for his fine computational work. They would also like to especially thank Professor M. Ishikawa at Université de Genève, and Professor Y. Muto and Mr. H. Iwasaki at Tohoku University for providing their experimental results prior to publication. This work was supported by grant aid from the Ministry of Education, Science and Culture, Japan, and by the Natural Science Engineering Research Council, Canada.

---

*Present address: The Research Institute for Iron, Steel and Other Metals, Tohoku University, Katahira, Sendai 980, Japan.

[1]See, for example, M. B. Maple, J. Phys. (Paris) 39, C6-1374 (1978).

[2]See, for example, M. Ishikawa and Ø. Fischer, J. Phys. (Paris) 39, C6-1379 (1978).

[3]See, for example, D. E. Moncton, G. Shirane,and W. Thomlinson, J. Magn. Magn. Mater. 14, 172 (1979).

[4]R. W. McCallum, D. C. Johnston, R. N. Shelton, and M. B. Maple, Solid State Commun. 24, 391 (1977).

[5]R. W. McCallum, D. C. Johnston, R. N. Shelton, W. A. Fertig, and M. B. Maple, Solid State Commun. 24, 501 (1977).

[6]M. Ishikawa and Ø. Fischer, Solid State Commun. 24, 747 (1977).

[7]M. Ishikawa and J. Muller, Solid State Commun. 27, 761 (1978).

[8]J. W. Lynn, D. E. Moncton, G. Shirane, W. Thomlinson, J. Eckert, and R. N. Shelton, J. Appl. Phys. 49, 1389 (1978).

[9]D. E. Moncton, G. Shirane, W. Thomlinson, M. Ishikawa, and Ø. Fischer, Phys. Rev. Lett. 41, 1133 (1978).

[10]C. F. Majkrzak, G. Shirane, W. Thomlinson, M. Ishikawa, Ø. Fischer, and D. E. Moncton, Solid State Commun. 31, 773 (1979).

[11]W. Thomlinson, G. Shirane, D. E. Moncton, M. Ishikawa, and Ø. Fischer, J. Appl. Phys. 50, 1981 (1979).

[12]H. C. Hamaker, L. D. Woolf, H. B. MacKay, Z. Fisk, and M. B. Maple, Solid State Commun. 31, 139 (1979).

[13]H. C. Hamaker, L. D. Woolf, H. B. MacKay, Z. Fisk, and M. B. Maple, Solid State Commun. 32, 289 (1979).

[14]W. Thomlinson, G. Shirane, D. E. Moncton, M. Ishikawa, and Ø. Fischer, Phys. Rev. B (in press).

[15]W. A. Fertig, D. C. Johnston, L. E. DeLong, R. W. McCallum, M. B. Maple, and B. T. Matthias, Phys. Rev. Lett. 38, 987 (1977).

[16]D. E. Moncton, D. B. McWhan, J. Eckert, G. Shirane, and W. Thomlinson, Phys. Rev. Lett. 39, 1164 (1977).

[17]D. E. Moncton, D. B. McWhan, P. H. Schmidt, G. Shirane, W. Thomlinson, M. B. Maple, H. B. MacKay, L. D. Woolf, Z. Fisk, and D. C. Johnston, Phys. Rev. Lett.

45, 2060 (1980).
[18]M. Ishikawa and Ø. Fischer, Solid State Commun. 23, 37 (1977).
[19]J. W. Lynn, D. E. Moncton, W. Thomlinson, G. Shirane, and R. N. Shelton, Solid State Commun. 26, 493 (1978).
[20]J. W. Lynn, G. Shirane, W. Thomlinson, and R. N. Shelton, Phys. Rev. Lett. 46, 368 (1981).
[21]J. W. Lynn, J. L. Ragazzoni, R. Pynn, and J. Joffrin, J. Phys. (Paris) Lett. 42, L45 (1981).
[22]D. Rainer, Z. Phys. 252, 174 (1972).
[23]S. Maekawa and M. Tachiki, Phys. Rev. B 18, 4688 (1978); S. Maekawa, M. Tachiki, and H. Kurita, J. Phys. (Paris) 39, C6-377 (1978).
[24]C. Y. Huang, S. E. Kohn, S. Maekawa, and J. L. Smith, Solid State Commun. 32, 929 (1979).
[25]A. Sakurai, Solid State Commun. 25, 867 (1978).
[26]K. Machida and D. Youngner, J. Low Temp. Phys. 35, 449 (1979); 35, 561 (1979); D. Younger and K. Machida, *ibid.* 36, 617 (1979).
[27]K. Machida, J. Low Temp. Phys. 37, 583 (1979).
[28]H. Suhl, J. Less Common Met. 62, 225 (1978).
[29]T. K. Lee, Yu. A. Izyumov, and J. L. Birman, Phys. Rev. B 20, 4494 (1979); T. K. Lee, Solid State Commun. 34, 9 (1980).
[30]N. R. Werthamer, E. Helfand, and P. C. Hohenberg, Phys. Rev. 147, 295 (1966).
[31]K. Maki, Phys. Rev. 148, 362 (1966).
[32]N. Sano, T. Taniguchi, and K. Asayama, Solid State Commun. 33, 419 (1980).
[33]P. W. Anderson, Phys. Rev. Lett. 3, 325 (1959).
[34]A. A. Abrikosov and L. P. Gor'kov, Sov. Phys. JETP 15, 752 (1962) [Zh. Eksp. Teor. Fiz. 42, 1088 (1962)].
[35]T. Jarlborg, A. J. Freeman, and T. J. Watson-Yang, Phys. Rev. Lett. 39, 1032 (1977); T. Jarlborg and A. J. Freeman, *ibid.* 44, 178 (1980).
[36]M. Redi and P. W. Anderson, Bull. Am. Phys. Soc. 24, 389 (1979).
[37]U. Krey, Int. J. Magn. 3, 65 (1972); 4, 153 (1973).
[38]M. V. Jarić and M. Belić, Phys. Rev. Lett. 42, 1015 (1979).
[39]H. Matsumoto, H. Umezawa, and M. Tachiki, Solid State Commun. 31, 157 (1979); M. Tachiki, A. Kotani, H. Matsumoto, and H. Umezawa, *ibid.* 31, 927 (1979).
[40]E. I. Blount and C. M. Varma, Phys. Rev. Lett. 42, 1079 (1979); H. S. Greenside, E. I. Blount, and C. M. Varma, *ibid.* 46, 49 (1981).
[41]M. Tachiki, H. Matsumoto, T. Koyama, and H. Umezawa, Solid State Commun. 34, 19 (1980); O. Sakai, M. Tachiki, H. Matsumoto, and H. Umezawa, *ibid.* 39, 279 (1981).
[42]C. G. Kuper, M. Revzen, and A. Ron, Phys. Rev. Lett. 44, 1545 (1980); Solid State Commun. 36, 533 (1980).
[43]M. Tachiki, A. Kotani, H. Matsumoto, and H. Umezawa, Solid State Commun. 32, 599 (1979); M. Tachiki, S. Takahashi, H. Matsumoto, and H. Umezawa, *ibid.* 35, 393 (1980).
[44]M. Tachiki, A. Kotani, S. Takahashi, T. Koyama, H. Matsumoto, and H. Umezawam, Solid State Commun. 37, 113 (1981); A. Kotani, S. Takahashi, M. Tachiki, H. Matsumoto, and H. Umezawa, *ibid.* 37, 619 (1981).
[45]M. Tachiki, in *Proceedings of the International Conference on Ternary Superconductors, Lake Geneva, Wisconsin, 1980* (North-Holland, Amsterdam, 1981), p. 267.
[46]M. Tachiki, H. Matsumoto, and H. Umezawa, Phys. Rev. B 20, 1915 (1979).
[47]T. Krzyszton, J. Magn. Magn. Mater. 15, 1572 (1980).
[48]See, for example, J. Kanamori, in *Magnetism III,* edited by G. T. Rado and H. Suhl (Academic, New York and London, 1963), p. 127.
[49]M. Tachiki, T. Koyama, H. Matsumoto, and H. Umezawa, Solid State Commun. 34, 269 (1980).
[50]S. Maekawa, M. Tachiki, and S. Takahashi, J. Magn. Magn. Mater. 13, 324 (1979).
[51]M. Pelizzone, A. Treyvaud, P. Spitzli, and Ø. Fischer, J. Low Temp. Phys. 29, 453 (1977).
[52]Y. Muto, H. Iwasaki, T. Sasaki, N. Kobayashi, M. Ikebe, and M. Isino, in Ref. 45; H. Iwasaki, M. Isino, and Y. Muto (private communication).
[53]H. Adrian, K. Müller, and G. Saemann-Ischenko, Phys. Rev. B 22, 4424 (1980).
[54]P. W. Anderson and H. Suhl, Phys. Rev. 116, 898 (1959).
[55]A. A. Abrikosov and L. P. Gor'kov, Sov. Phys. JETP 12, 1243 (1961) [Zh. Eksp. Theor. Fiz. 39, 1781 (1960)].
[56]W. Baltensperger and S. Strässler, Phys. Konden. Mater. 1, 20 (1963); P. Petalas and W. Baltensperger, Helv. Phys. Acta 41, 388 (1968).
[57]K. Machida and T. Matsubara, Solid State Commun. 31, 791 (1979); J. Phys. Soc. Jpn. 48, 799 (1980).
[58]K. Machida, K. Nokura, and T. Matsubara, Phys. Rev. Lett. 44, 821 (1980); Phys. Rev. B 22, 2307 (1980).
[59]M. J. Nass, K. Levin, and G. S. Grest, Phys. Rev. Lett. 46, 614 (1981).
[60]L. D. Woolf, D. C. Johnston, H. B. MacKay, R. W. McCallum, and M. B. Maple, J. Low Temp. Phys. 35, 651 (1979).